Conformational Properties of Cylindrical Rod Brushes Consisting of a Polystyrene Main Chain and Poly(*n*-hexyl isocyanate) Side Chains

Moriya Kikuchi,[†,§] Le Thi Ngoc Lien,[†] Atsushi Narumi,[†] Yuji Jinbo,[‡] Yoshinobu Izumi,[‡] Katsutoshi Nagai,[†] and Seigou Kawaguchi*[,†]

Department of Polymer Science and Engineering, Graduate School of Science and Engineering, Yamagata University, 4-3-1 Jonan, Yonezawa 992-8510, Japan, and Graduate Program of Human Sensing and Functional Sensor Engineering, Graduate School of Science and Engineering, Yamagata University, 4-3-16 Jonan, Yonezawa 992-8510, Japan

Received April 28, 2008; Revised Manuscript Received July 9, 2008

ABSTRACT: Conformational properties of cylindrical rod brushes consisting of a flexible polystyrene main chain and poly(*n*-hexyl isocyanate) (PHIC) rod side chains have thoroughly been studied by static light and small-angle X-ray scattering (SAXS) in tetrahydrofuran (THF) at 25 °C. These rod brushes were prepared by radical homopolymerization of 4-vinylbenzyloxy-ended PHIC macromonomers (**1**) (VB-HIC-N_s, where N_s is the weight-averaged degree of polymerization of HIC and in a range from 21 to 80) in *n*-hexane at 60 °C. The mean-square cross-sectional radius of gyration ($\langle R_c^2\rangle_0$) of the brush at an infinite dilution is determined by SAXS measurement and rationalized as a function of N_s. The experimental value of $\langle R_c^2\rangle_0$ gradually increases with N_s but above N_s higher than 20 increases to follow the scaling law of $\langle R_c^2\rangle_0 \propto N_s^{0.87}$. The experimental N_s dependence of $\langle R_c^2\rangle_0$ is compared to that from the wormlike comb model whose main and side chains have different stiffness parameters. The molecular weight dependence of *z*-averaged mean-square radius of gyration ($\langle R_g^2\rangle_z$) of the brush is determined and analyzed in terms of the wormlike cylinder model taking into account the end effects. The parameters characteristic of the rod brush in THF solution, such as the main chain stiffness parameter (λ_M^{-1}), the molecular weight per unit contour length (M_L), and the excluded-volume strength (B), are determined and rationalized as a function of the contour length of the side rod. The polystyrene main chain stiffness of the rod brush remarkably increases by the densely located rod side chains to follow the scaling law of $\lambda_M^{-1} \propto N_s^1$. The backbone stiffness of the rod brush is higher than that of the flexible brush consisting of flexible polystyrene side chains with the corresponding contour length. A single rod brush of poly(VB-HIC-47) deposited on a mica surface is observed by the scanning force microscopy to reasonably demonstrate the cylindrical rod brushes.

Introduction

Since an initial report by Schmidt and Tsukahara et al.[1] in 1994, poly(macromonomer)s, bottle brush macromolecules, or cylindrical polymer brushes, which have one of the best defined comb-branching architecture, have attracted considerable attention. A number of brush polymers consisting of flexible polymer main and side chains have so far been prepared, including polystyrene,[2−11] poly(methyl methacrylate),[12] poly(ethylene oxide),[13−15] poly(*N*-isopropylacrylamide),[16] poly(*n*-butyl acrylate),[17] core−shell brushes of block copolymers of styrene with 2-vinylpyridine,[18] and ε-caprolactone with *n*-butyl acrylate.[19] Recent great progress in the controlled living radical polymerization allows one to prepare those brushes by the "grafting from" method. One interesting and very valuable finding in conformational properties of the brushes with the regular comb-branching structure is that the main chain remarkably stiffens in a dilute solution and solid state, despite being originally composed of flexible chains. The main chain stiffness parameter (λ_M^{-1}) in the wormlike cylinder model increases with increasing side chain length and solvent power.[1,3,4,6−9,12,13] The theoretical studies[9,21,22] have also demonstrated that such stiffening effects may be reasonably considered to arise from repulsive interactions (excluded-volume effect) among the side chains.

Cylindrical brushes, however, are limited to those consisting of flexible main and side polymer chains in solution. Little experimental work is known about brushes consisting of semiflexible or rodlike polymer side chains, except for Monte Carlo simulation.[23] The simulation results demonstrated that the main chain stiffness of the rod brush with a relatively low grafting density is much higher than the flexible brush with the same side contour length. The theoretical study based on the mean-field approach showed that the $\lambda_M^{-1}$of the main chain of the rod brush may be proportional to $L_s^2/\ln(L_s)$, where L_s is the contour length of the side rod.[24] It may be quite essential and interesting from the experimental point of view, therefore, to clarify how the side chain flexibilities affect their main chain stiffness. Recently, Schmidt et al.[25] have prepared the cylindrical rod brushes consisting of poly(L-lysine) and poly(L-glutamate) side chains by "grafting through" or "grafting from" techniques. They demonstrated from the scanning force microscopy (SFM) observation that the main chain stiffness increases by the rod side chains. Unfortunately, since the grafting density was incomplete (about 40−50%) by the "grafting from" method and weight-averaged degree of polymerization of the main chain (N_M) was very low (N_M is ca. 4) by the "grafting through" (macromonomer) method, they did not report any parameters characterizing the conformation of the rod brush in solution.[25]

Polyisocyanates are thought to be a candidate as a rodlike side chain because they are well-known to be one of the representative semiflexible polymers in solution. Among others, poly(*n*-hexyl isocyanate) (PHIC) is the best characterized polyisocyanates. It assumes a dynamic 8_3 helical conformation with the stiffness parameter $\lambda^{-1} = 84$ nm and the molecular weight per unit contour length of $M_L = 730$ g mol^{-1} nm^{-1} in *n*-hexane at 25 °C.[26]

We have recently reported the syntheses of 4-vinylbenzyloxy- and 2-methacryloyloxyethoxy-ended rodlike PHIC macromono-

* To whom correspondence should be addressed: e-mail skawagu@yz.yamagata-u.ac.jp; Fax 81- 238-26-3182.
† Department of Polymer Science and Engineering.
‡ Graduate Program of Human Sensing and Functional Sensor Engineering.
§ Present address: Institute for Materials Chemistry and Engineering. Kyushu University, 744 Motooka, Nishi-ku, Fukuoka 819-0395, Japan.

10.1021/ma800951d CCC: $40.75
Published on Web 08/16/2008

Scheme 1. Reaction for Cylindrical Rod Brush Using PHIC Rodlike Macromonomer

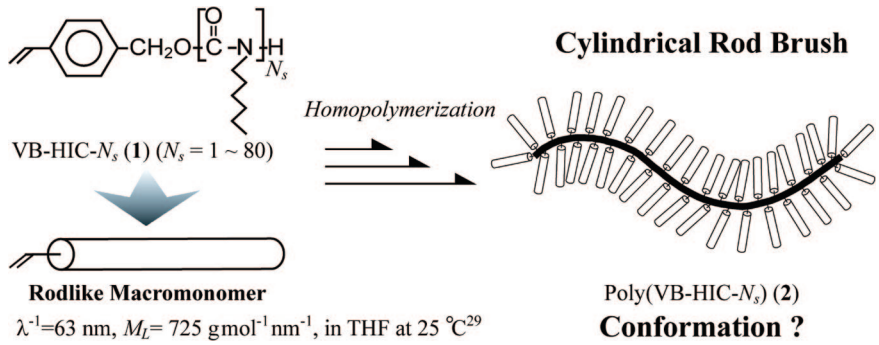

Table 1. Characteristics of VB-HIC-N_s Macromonomers

VB-HIC-N_s	$M_w \times 10^3$ [b] (g mol^{-1})	N_s [d]	M_w/M_n [b]
VB-BIC-1[a]	0.23[c]	1	1.00
VB-HIC-21	2.81	21	1.1_9
VB-HIC-29	3.88	29	1.1_1
VB-HIC-32	4.21	32	1.1_2
VB-HIC-47	6.05	47	1.1_5
VB-HIC-62	8.04	62	1.1_6
VB-HIC-80	10.3	80	1.1_6

[a] *p*-Vinylbenzylbutylurethane. [b] Determined by SEC calibrated with a series of PHICs as a standard.[29] [c] Calculated from the molecular structure. [d] Weight-averaged degree of polymerization of HIC.

Table 2. Characteristics of Poly(VB-HIC-N_s) Samples Used in the SAXS Measurement and $\langle R_c^2\rangle_0^{1/2}$ Values

sample	$M_w \times 10^{-5}$ [b] (g mol^{-1})	M_w/M_n [b]	dn/dc [c] (mL/g)	$\langle R_c^2\rangle_0^{1/2}$ [d] (nm)
polystyrene	0.441	1.0_7	0.185_0	0.311
poly(VB-BIC-1)[a]	3.72	1.4_1	0.143	0.618
poly(VB-HIC-21)	6.17	1.5_2	0.092_7	2.28
poly(VB-HIC-29)	97.9	1.2_7	0.091_4	2.80
poly(VB-HIC-32)	8.05	1.4_2	0.089_8	3.34
poly(VB-HIC-47)	76.3	1.3_6	0.088_8	4.66
poly(VB-HIC-62)	8.39	1.4_4	0.088_7	5.80
poly(VB-HIC-80)	34.6	1.6_8	0.087_8	7.11

[a] Poly(*p*-vinylbenylbutylurethane). [b] Determined by SEC-MALS in THF at 25 °C. [c] In THF at 25 °C. [d] Determined by SAXS in THF at 25 °C.

mers (**1**) (VB-HIC-N_s and MA-HIC-N_s) and their fundamental radical copolymerization behavior.[27,28] In addition, many details for the molecular characterizations of VB-HIC-N_s as well as polymacromonomer, poly(VB-HIC-47) (**2**), in THF at 25 °C by small-angle X-ray scattering (SAXS), SEC-MALS, and viscosity measurements were reported.[29] The macromonomer and linear PHIC chain have been characterized by using the parameters $\lambda^{-1} = 63$ nm and $M_L = 725$ g mol^{-1} nm^{-1} in THF at 25 °C, implying that the macromonomer with M_w less than 2.45×10^4 g mol^{-1} is considered as a cylindrical rod.[29] Interestingly, the main chain stiffness of the rod brush, poly(VB-HIC-47), remarkably increased by the presence of densely located rod side chains, in accordance with the simulation results and theoretical prediction as mentioned above.

In the present paper, we report many details of the experimental works of the conformational properties of the PHIC rod brushes in THF at 25 °C by small-angle X-ray scattering (SAXS) and SEC-MALS, as shown in Scheme 1. Especially, we focus on the influence of side rod length on the main chain stiffness of the cylindrical rod brushes. Also, the comparison in main chain stiffness between the rod and flexible side chain brushes is presented and discussed.

Experimental Section

Materials. PHIC macromonomers (VB-HIC-N_s, where N_s is an weight-averaged degree of polymerization of HIC) were prepared by initiator method of living coordination polymerization of HIC using a titanium alkoxide complex (IV) as an initiator. The details of the preparation and characterization of the macromonomers were described in the previous papers.[27−29] Characterization of the macromonomers was carried out by SEC measurement calibrated with a series of PHIC's as a standard.[29] Characteristics of the macromonomers used in this study are listed in Table 1. The polymacromonomer samples, poly(VB-HIC-N_s), were prepared by the radical homopolymerization of VB-HIC-N_s using dimethyl-2,2′-azobis(2-methyl propionate) (V-601) as an initiator in *n*-hexane at 60 °C for 24 h. After polymerization, the reaction mixtures were dissolved into benzene and freeze-dried, followed by washing with *n*-hexane to remove unreacted (unpolymerized) macromonomer. One interesting experimental observation to be noted here is in the solubility of the rod brushes; i.e., PHIC macromonomer is soluble in *n*-hexane but the rod brush with high N_M is not at room temperature, whereas the chemical composition of PHIC in the brush is extremely high. This may be remarkably different from that of the conventional flexible brushes. In the latter, the solubility of the brushes may be determined by, or similar to that of, the parent macromonomer. The difference in the solubility between flexible and rod brushes is most likely due to the low configurational entropic contribution of the side rod chains to the mixing. About 98% of the unreacted macromonomer could be removed by the procedure. To completely remove the unreacted macromonomer, the products were further fractionated by repeating fractional precipitations with toluene as a solvent and acetonitrile as a precipitant.

Measurements. Weight-averaged molecular weight (M_w) and *z*-averaged mean-square radius of gyration ($\langle R_g^2\rangle_z$) of the polymacromonomer were determined by a SEC-MALS (eluent: THF; flow rate: 1.0 mL/min; 40 °C; columns: Shodex KF802 + KF806L + KF806L, RI; Shodex RI-101, UV; Tosoh UV-8020), equipped with a multiangle light scattering detector (MALS; Wyatt Technology DAWN-DSP, wavelength $\lambda = 632.8$ nm) at room temperature of 25 °C. The Rayleigh ratio $R(90)$ at a scattered angle of 90° was based on that of pure toluene at wavelength of 632.8 nm at 25 °C. The corrections for sensitivity of 17 detectors at angles of other than 90° and dead volume for each detector were performed using the scattering intensities of 0.30 wt % THF solution of polystyrene standard with $M_w = 1.88 \times 10^4$ g mol^{-1} and $M_w/M_n = 1.0_3$. Polymer sample solutions with mass concentration (C_p) of about 5×10^{-4} g/mL were injected using a sample loop of 100 μL to SEC columns and diluted down to $10-10^3$ times lower than original C_p in the columns during the separation. Thus, the concentration effect on the value of M_w and $\langle R_g^2\rangle_z$ can be ignored.

The specific refractive index increment (dn/dc) for the polymacromonomers in THF at 25 °C was measured using a differential refractometer (Otsuka Electronics DRM-1021, wavelength $\lambda =$ 632.8 nm) and listed in Table 2. Sample solutions were prepared by gravimetric method. The weight fraction, W_p, is then converted to C_p (g/mL) by

$$C_p\,(\mathrm{g/mL}) = \frac{W_p}{\rho_0^{-1}(1 - W_p) + \nu W_p} \qquad (1)$$

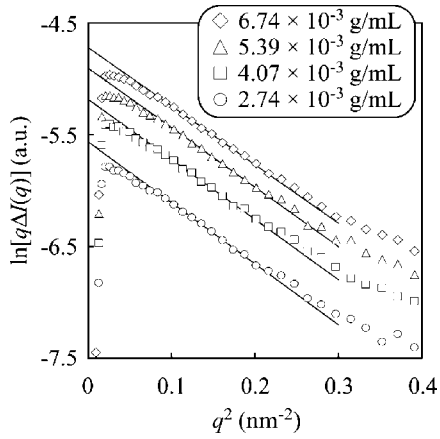

Figure 1. Cross-section Guinier plots of $\ln[q\Delta I(q)]$ as a function q^2 for poly(VB-HIC-32) in THF at 25 °C.

where ρ_0 is the density of pure solvent (0.8830 g/mL for THF at 25 °C) and ν is the partial specific volume of PHIC (1.00 mL/g for THF at 25 °C[29]).

Small-angle X-ray scattering (SAXS) measurement was carried out at 25 °C, using BL-10C with a synchrotron orbital radiation as an X-ray source set up in the Photon Factory of the High Energy Accelerator Organization at Tsukuba, Ibaraki, Japan. The wavelength of the X-rays was 1.488 Å. The scattered intensity was recorded by a position-sensitive proportional counter (PSPC) with 512 channels over a scattering vector range from 0.02 to 0.30 Å^{-1}. The scattered vector was calibrated using a sixth peak of dry collagen.

Results and Discussion

We first report the dimensional properties of the cross-sectional radius of gyration of the rod brushes in THF at 25 °C. Second, the global dimensional properties of the rod brushes are reported and compared with those of the flexible brushes.

Cross-Sectional Radius of Gyration of Rod Comb. Figure 1 shows typical examples of cross-section Guinier plots of $\ln[q\Delta I(q)]$ obtained by SAXS measurement versus q^2 for poly(VB-HIC-32) ($M_w = 8.05 \times 10^5$ g mol^{-1}, $M_w/M_n = 1.4_2$) in THF at 25 °C at various C_p's. The cross-section radius of gyration ($\langle R_c^2\rangle^{1/2}$) may be determined via the following equation:[30]

$$\ln[q\Delta I(q)] = \ln \frac{k^2 N\pi}{L} - \frac{1}{2}\langle R_c^2\rangle q^2 \qquad (2)$$

Here $\Delta I(q)$ is the experimental excess scattering intensity, L the contour length of the cylinder, k the electron density contrast factor, N the number of cylinder, and q the scattering vector as defined with the scattering angle of θ and the wavelength λ by

$$q = \frac{4\pi \sin\theta}{\lambda} \qquad (3)$$

Figure 2 shows C_p dependence of $\langle R_c^2\rangle^{1/2}$ for the rod brushes with different side chain lengths in THF at 25 °C. The experimental data for linear polystyrene (PSt, $M_w = 4.41 \times 10^4$ g mol^{-1}, $M_w/M_n = 1.0_7$) and poly(*p*-vinylbenzylbutylurethane) (poly(VB-BIC-1)) in THF at 25 °C are also shown in this figure for comparison. By extrapolating to $C_p = 0$, one obtains $\langle R_c^2\rangle^{1/2}$ of a brush at an infinite dilution, and these values are summarized in Table 2.

The N_s dependence of $\langle R_c^2\rangle_0^{1/2}$ is shown in Figure 3a. One sees in this figure that in the region of $N_s < 10$ the experimental value of $\langle R_c^2\rangle_0^{1/2}$ gradually increases with N_s, but above it the slope in the plot of log $\langle R_c^2\rangle_0^{1/2}$ with log N_s increases with N_s and then approaches a constant value. By the least-squares

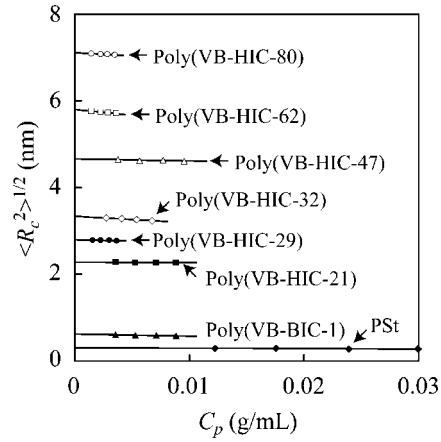

Figure 2. Cross-section radius of gyration $\langle R_c^2\rangle^{1/2}$ as a function of C_p for polystyrene, poly(VB-BIC-1), and poly(VB-HIC-N_s) in THF at 25 °C.

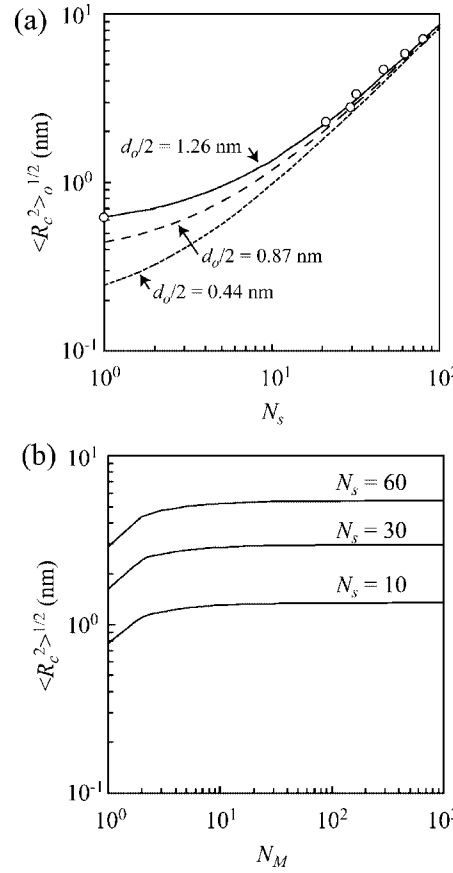

Figure 3. (a) N_s dependence of the measured $\langle R_c\rangle_0^{1/2}$ for poly(VB-HIC-N_s) and poly(VB-BIC-1) in THF at 25 °C. The solid line is calculated by eqs 5−8 with $d_0/2 = 1.26$ nm and $l_M = 0.22$ nm. The broken and dotted lines are ones with $d_0/2 = 0.87$ and 0.44 nm, respectively. (b) N_M dependence of $\langle R_c\rangle^{1/2}$ calculated from eqs 5−8 with $d_0/2 = 1.26$ nm and $l_M = 0.22$ nm.

method for experimental data of the brushes with N_s higher than 20, one obtains the following relation between $\langle R_c^2\rangle_0^{1/2}$ and N_s, within the present experimental N_s range:

$$\langle R_c^2\rangle_0^{1/2} \propto N_s^{0.87} \qquad (4)$$

This power law exponent of 0.87 is much higher than that of the flexible brushes consisting of a polymethacrylate main chain and flexible PSt side chains. In the latter brushes, the values of 0.61−0.67 in toluene and 0.56 in cyclohexane were reported.[4]

The high exponent value closely suggests the rod brushes with the rod as a side chain. To account this high exponent in the present rod brushes, the experimental data are compared to those calculated from the wormlike comb model whose main and side chains have different stiffness parameters, λ_M^{-1} and λ_s^{-1}, respectively.[31] Each side chain of contour length L_s is linked to the main chain of contour length $N_M l_M$ by a universal joint, where N_M is the weight-averaged degree of polymerization of the main chain ($N_M = M_w/M_{macromonomer}$, where $M_{macromonomer}$ is the M_n of the macromonomer) and l_M is the contour length per backbone monomer. According to this model, $\langle R_c^2 \rangle$ may be given by[31]

$$\langle R_c^2 \rangle = \frac{N_M}{L_T^2} \times \left\{ L_s^2 \left[\frac{L_s}{6\lambda_s} - \frac{1}{4\lambda_s^2} + \frac{1}{4\lambda_s^3 L_s} - \frac{1}{8\lambda_s^4 L_s^2}(1 - \exp(-2\lambda_s L_s)) \right] + L_s(L_T - L_s) \left[\frac{L_s}{2\lambda_s} - \frac{1}{2\lambda_s^2} + \frac{1}{4\lambda_s^3 L_s}(1 - \exp(-2\lambda_s L_s)) \right] \right\} \quad (5)$$

where L_T is the total contour length of the brush, which is given by

$$L_T = N_M L_s + (N_M - 1) l_M \quad (6)$$

The side chain contour length, L_s, may be assumed as the sum of the PHIC side contour and main chain thickness ($d_0/2$), which is given by

$$L_s = L_{PHIC} + \frac{d_0}{2} \quad (7)$$

Here L_{PHIC} is the contour length of PHIC ($L_{PHIC} = (N_s M_0)/M_L$) with M_0 being the molecular weight of HIC and $M_L = 725$ g mol^{-1} nm^{-1} in THF at 25 °C,[29] and d_0 is the diameter of the main chain. Since L_s is nearly equal to λ_s for the rod comb with large N_s, eq 5 may be simplified to

$$\langle R_c^2 \rangle = \frac{N_M L_s^3}{L_T^2} \left(\frac{L_s}{6} + \frac{2L_T - 3L_s}{8}(1 - e^{-2}) \right) \quad (8)$$

In Figure 3b, the values of $\langle R_c^2 \rangle^{1/2}$ calculated using eqs 6−8 with $l_M = 0.22$ nm and $d_0/2 = 1.26$ nm for $N_s = 10$, 30, and 60 are plotted against N_M. It can be seen that the calculated value of $\langle R_c^2 \rangle^{1/2}$ steeply increases with increasing N_M and approaches the constant value at N_M higher than 10^2. It should be worthwhile to say here that the calculated value of $\langle R_c^2 \rangle^{1/2}$ is not sensitive to the l_M value used. The value of l_M will be experimentally determined from the global conformational properties of the brushes and described later. The calculated value of $\langle R_c^2 \rangle^{1/2}$ at $N_M = 10^4$ was tabulated as a function of N_s and compared to the experimental data, as shown in Figure 3a. The calculated curve (solid line) seems to fairly explain the experimental N_s dependence of $\langle R_c^2 \rangle_0^{1/2}$ to demonstrate that the brush consists of the rods. Two comments on the comparison of the experiment with the theory are worth mentioning. First is the difference in the electron density contrast factor between main and side chains. In the wormlike comb model as mentioned above, this effect is ignored. The electron density contrast of the main chain, poly(*p*-oxymethylstyrene), and side chain, HIC, to THF at 25 °C is calculated to be 2.61×10^{22} and 3.65×10^{22} electrons/mL, respectively. Therefore, at $N_s = 1.0$ there is about 14% contrast difference between main and side chain. At N_s higher than 10, however, the difference is less than 2%, and the influence of the contrast difference on the experimental value of $\langle R_c^2 \rangle_0^{1/2}$ can be neglected. Second is the value of $d_0/2$. The actual main chain of the present brush is the poly(*p*-oxymethylstyrene). The value of $d_0/2 = 1.26$ nm assumed in the calculation seems to be somewhat higher than the value ($d_0/2 = 0.44$ nm) calculated from the $\langle R_c^2 \rangle_0^{1/2}$ for linear PSt and $d_0/2 = 0.87$ nm from the $\langle R_c^2 \rangle_0^{1/2}$ for poly(VB-BIC-1) in Table 2. The influence of the value of $d_0/2$ on the calculated value is investigated, and the calculated values with $d_0/2 = 0.44$ nm (dotted line) and $d_0/2 = 0.87$ nm(broken lines) are also shown in Figure 3a. One sees that in the region of N_s smaller than 20, the calculated curves considerably deviate downward from the experimental data with decrease of the $d_0/2$ value used, implying that the calculated ones are very sensitive to the $d_0/2$ value in the low N_s region. In the region of N_s larger than 20, however, the calculated values are not so sensitive to the $d_0/2$ value and at least qualitatively describe the experimental data.

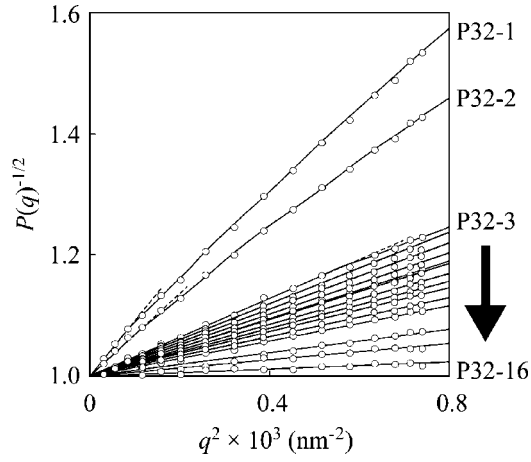

Figure 4. Angular dependence of $P(q)^{-1/2}$ for the indicated fractions of poly(VB-HIC-32) in THF at 25 °C by SEC-MALS. The broken lines indicate an initial slope.

Global Conformation of Rod Brushes. Figure 4 shows the root plots of $P(q)^{-1/2}$ versus q^2 for poly(VB-HIC-32) determined by SEC-MALS in THF at 25 °C, where $P(q)$ denotes the single particle scattering function. From the initial slope (denoted by broken line) in these plots, one determines the mean-square radius of gyration $\langle R_g^2 \rangle_z^{1/2}$ of the rod brush in THF at 25 °C via the following equation:

$$P(q)^{-1/2} = 1 + \frac{1}{6}\langle R_g^2 \rangle_z q^2 \quad \text{and} \quad q = \frac{4\pi n_0 \sin(\theta/2)}{\lambda} \quad (9)$$

where n_0 is the refractive index of THF. The molecular characteristics of the poly(VB-HIC-N_s) from $N_s = 21$ to 80 in THF at 25 °C are listed in Tables 3, 4, 5, and 6.

Figure 5 shows the double-logarithmic plot of $\langle R_g^2 \rangle_z^{1/2}$ versus the weight-averaged degree of polymerization of the main chain N_M for poly(VB-HIC-32) in THF at 25 °C, together with the data of linear PSt in THF at 25 °C given by the following equation:[31]

$$\langle R_g^2 \rangle_z^{1/2} = 1.18 \times 10^{-2} M_w^{0.6} \text{ (nm)} \quad (10)$$

It should be noted that $\langle R_g^2 \rangle_z^{1/2}$ of the poly(VB-HIC-32) is much larger than that of linear PSt with the corresponding N_M. This clearly implies that the PSt main chain stiffness of the poly(VB-HIC-32) is much higher than that of the linear PSt in THF at 25 °C. In other words, the main chain of the rod brush remarkably stiffens by the densely located stiff rods.

Table 3. Characterization Results on Poly(VB-BIC-1) and Poly(VB-HIC-21)

sample		$M_w \times 10^{-6}$ [a] (g mol^{-1})	$N_M \times 10^{-3}$ [b]	$\langle R_g^2\rangle_z^{1/2}$ (nm)
$N_s = 1$	P1-1	1.57	6.74	47.0
	P1-2	1.30	5.57	40.7
	P1-3	0.937	4.02	33.3
	P1-4	0.659	2.83	27.3
	P1-5	0.421	1.81	21.4
	P1-6	0.250	1.07	16.3
$N_s = 21$	P21-1	4.13	1.75	38.8
	P21-2	3.09	1.17	32.8
	P21-3	2.76	1.31	30.6
	P21-4	2.47	1.05	28.6
	P21-5	2.37	1.00	27.8
	P21-6	2.20	0.930	26.7
	P21-7	1.99	0.843	25.3
	P21-8	1.84	0.780	24.1
	P21-9	1.67	0.706	22.7
	P21-10	1.47	0.624	21.2
	P21-11	1.08	0.456	17.6
	P21-12	0.637	0.270	12.9

[a] Determined by SEC-MALS in THF at 25 °C. [b] Weight-averaged degree of polymerization of the main chain, $N_M = M_w/M_{macromomomer}$, where $M_{macromonomer}$ is the M_n of the macromonomer.

Table 4. Characterization Results on Poly(VB-HIC-29)

sample		$M_w \times 10^{-7}$ [a] (g mol^{-1})	$N_M \times 10^{-3}$ [b]	$\langle R_g^2\rangle_z^{1/2}$ (nm)
$N_s = 29$	P29-1	1.61	4.61	70.3
	P29-2	1.14	3.27	57.9
	P29-3	0.645	1.85	42.2
	P29-4	0.370	1.06	31.2
	P29-5	0.329	0.940	29.1
	P29-6	0.323	0.924	28.8
	P29-7	0.292	0.834	27.3
	P29-8	0.281	0.804	26.7
	P29-9	0.249	0.714	24.9
	P29-10	0.244	0.697	24.6
	P29-11	0.222	0.635	23.3
	P29-12	0.172	0.493	20.4
	P29-13	0.140	0.400	18.2
	P29-14	0.108	0.308	15.4

[a] Determined by SEC-MALS in THF at 25 °C. [b] Weight-averaged degree of polymerization of the main chain, $N_M = M_w/M_{macromomomer}$, where $M_{macromonomer}$ is the M_n of the macromonomer.

Table 5. Characterization Results on Poly(VB-HIC-32)

sample		$M_w \times 10^{-7}$ [a] (g mol^{-1})	$N_M \times 10^{-3}$ [b]	$\langle R_g^2\rangle_z^{1/2}$ (nm)
$N_s = 32$	P32-1	1.43	3.80	74.0
	P32-2	1.10	2.93	63.9
	P32-3	0.581	1.55	44.3
	P32-4	0.534	1.42	42.1
	P32-5	0.498	1.33	40.5
	P32-6	0.465	1.24	39.0
	P32-7	0.444	1.18	37.9
	P32-8	0.430	1.14	37.1
	P32-9	0.397	1.05	35.5
	P32-10	0.371	0.986	34.1
	P32-11	0.347	0.924	32.9
	P32-12	0.313	0.832	30.9
	P32-13	0.289	0.770	29.6
	P32-14	0.205	0.544	24.1
	P32-15	0.151	0.401	20.2
	P32-16	0.0754	0.201	13.2

[a] Determined by SEC-MALS in THF at 25 °C. [b] Weight-averaged degree of polymerization of the main chain, $N_M = M_w/M_{macromonomer}$, where $M_{macromonomer}$ is the M_n of the macromonomer.

Another interesting point to be noted in this figure is to show an S-shaped dependence of $\langle R_g^2\rangle_z^{1/2}$ on N_M, implying that the simple Kratky−Porod (KP) chain model is not applicable to describe the dependence.

Table 6. Characterization Results on Poly(Vb-HIC-62) and Poly(VB-HIC-80)

sample		$M_w \times 10^{-6}$ [a] (g mol^{-1})	$N_M \times 10^{-3}$ [b]	$\langle R_g^2\rangle_z^{1/2}$ (nm)
$N_s = 62$	P62-1	11.6	1.67	56.0
	P62-2	10.2	1.46	51.6
	P62-3	8.25	1.19	45.9
	P62-4	6.46	0.932	39.8
	P62-5	4.86	0.701	33.6
	P62-6	3.40	0.491	27.1
	P62-7	1.58	0.227	17.9
	P62-8	0.870	0.125	13.4
$N_s = 80$	P80-1	16.4	1.80	68.8
	P80-2	11.0	1.24	52.1
	P80-3	6.48	0.730	38.0
	P80-4	3.93	0.443	28.5
	P80-5	2.44	0.274	22.1
	P80-6	1.29	0.145	16.6

[a] Determined by SEC-MALS in THF at 25 °C. [b] Weight-averaged degree of polymerization of the main chain, $N_M = M_w/M_{macromonomer}$, where $M_{macromonomer}$ is the M_n of the macromonomer.

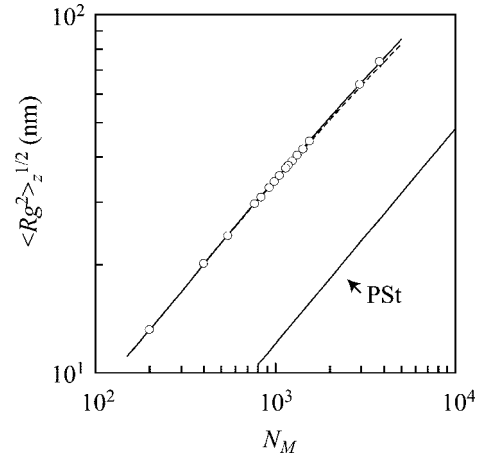

Figure 5. N_M dependence of the measured $\langle R_g^2\rangle_z^{1/2}$ for poly(VB-HIC-32) in THF together with that for linear PSt in THF at 25 °C.[31] The broken and solid lines are the theoretical values for the unperturbed and perturbed wormlike cylinder model with the parameters listed in Table 7.

One analyzes the N_M dependence of $\langle R_g^2\rangle_z^{1/2}$ for poly(VB-HIC-32), based on the cylindrical wormlike chain model with an end effect.[29] This situation is schematically shown in Figure 6, in which $\delta/2$ stands for the contribution of side chains near the ends to the main chain contour. The main chain contour length L_M may be given by

$$L_M = \frac{M_w}{M_L} + \delta \tag{11}$$

The mean-square radius of gyration ($\langle R_g^2\rangle$) of a cylindrical wormlike chain may be expressed by[32]

$$\langle R_g^2\rangle = \langle R_g^2\rangle_M + \langle R_c^2\rangle \tag{12}$$

where $\langle R_g^2\rangle_M$ is the main chain mean-square radius of gyration of a brush with a contour length L_M. According to Benoit and Doty for the Kratky−Porod chain,[33] the unperturbed $\langle R_g^2\rangle_M$ of a mondispersed wormlike chain with L_M is expressed by

$$\langle R_g^2\rangle_M = \frac{L_M}{6\lambda_M} - \frac{1}{4\lambda_M^2} + \frac{1}{4\lambda_M^3 L_M} - \frac{1}{8\lambda_M^4 L_M^2}[1 - \exp(-2\lambda_M L_M)] \tag{13}$$

Table 7. Cylindrical Wormlike Chain Parameters for Poly(VB-HIC-N_s) in THF

poly(VB-HIC-N_s)	λ_M^{-1} (nm)	$M_L \times 10^{-4}$ (g mol^{-1} nm^{-1})	$\langle R_c^2\rangle_0^{1/2}$ [c] (nm)	δ[d] (nm)	B (nm)
polystyrene	2.0[b]	0.0390[b]	0.311		
1[a]	(5.0 ± 1.0)	0.0926[e]	0.618		(0.6)
21	25	1.12	2.28	7.75	1.2
29	27	1.53	2.80	10.7	1.2
32	38	1.67	3.34	11.6	1.6
47	48	2.40	4.66	16.7	6.0
62	59	3.15[e]	5.80	22.2	
80	77	4.04[e]	7.11	28.4	

[a] Poly(*p*-vinylbenylbutylurethane). [b] Reference 40. [c] The same values as in Table 2. [d] Calculated from $\delta = 2L_{PHIC}$. [e] Calculated from $M_L = M_{macromonomer}/0.22$ nm^{-1}, where $M_{macromonomer}$ is the M_n of the macromonomer.

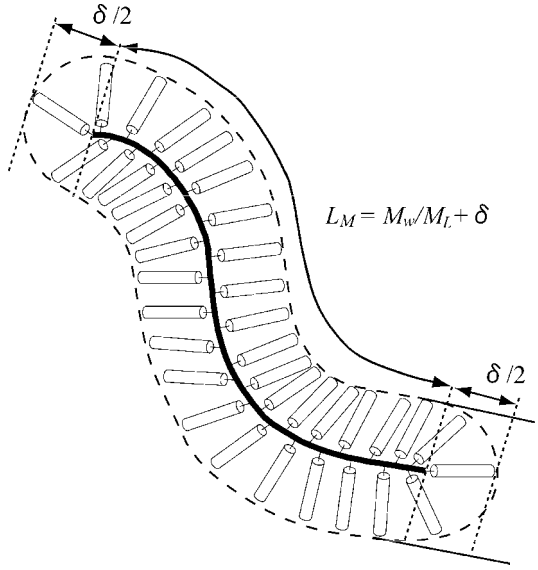

Figure 6. Schematic cartoon of the end effects of side chains (δ) near the ends on the main chain contour length of the rod brush.

Here, λ_M^{-1} is the main chain stiffness parameter (the Kuhn segment length). Equation 13 may also be approximated by[34]

$$\left(\frac{M}{\langle R_g^2\rangle_M}\right)^{1/2} = (6\lambda_M M_L)^{1/2}\left(1 + \frac{3M_L}{2}\left(\frac{1}{2\lambda_M} - \frac{\delta}{3}\right)\frac{1}{M}\right) \quad (14)$$

with the maximum error from the exact value being 2% for $\lambda_M L_M > 4$. Equation 14 indicates that $(M/\langle R_g^2\rangle_M)^{1/2}$ plotted against M^{-1} with $\delta = 2L_{PHIC}$ should give an upward curve, but within a limited region a straight line whose intercept and slope allow one the two parameters λ_M^{-1} and M_L to be evaluated.

Figure 7 shows the modified Murakami plots constructed from the experimental data ($\langle R_g^2\rangle_M = \langle R_g^2\rangle_z - \langle R_c^2\rangle_0$) for poly(VB-HIC-$N_s$) with $N_s = 21$, 29, and 32. The plots give an upward curve, but in $8 > \lambda_M L_M > 4$ the data follow a straight line (indicated in broken lines), which affords $\lambda_M^{-1} = 25$ nm and $M_L = 1.12 \times 10^4$ g mol^{-1} nm^{-1} for $N_s = 21$, $\lambda_M^{-1} = 27$ nm and $M_L = 1.53 \times 10^4$ g mol^{-1} nm^{-1} for $N_s = 29$, and $\lambda_M^{-1} = 38$ nm and $M_L = 1.67 \times 10^4$ g mol^{-1} nm^{-1} for $N_s = 32$. The solid lines in Figure 7 are the theoretical ones reconstructed from eq 14 with the parameters of λ_M^{-1} and M_L determined. The contour length per backbone monomer (l_M) calculated from $l_M = M_{macromonomer}/M_L$ for the rod brushes is ca. 0.22 nm, which is slightly smaller than the value for the polystyrene chain with the all-trans conformation.

Figure 5 shows the comparison of the experimental data of poly(VB-HIC-32) with the theoretical curve (broken line) calculated by using eqs 11−13 with the model parameters $\lambda_M^{-1} = 38$ nm, $M_L = 1.67 \times 10^4$ g mol^{-1} nm^{-1}, $\langle R_c^2\rangle_0^{1/2} = 3.34$ nm, and $\delta = 11.6$ nm. It can be seen that the experimental N_M dependence of $\langle R_g^2\rangle_z$ in the region of N_M less than 10^3 is quantitatively described by the wormlike cylinder model with the end effect.

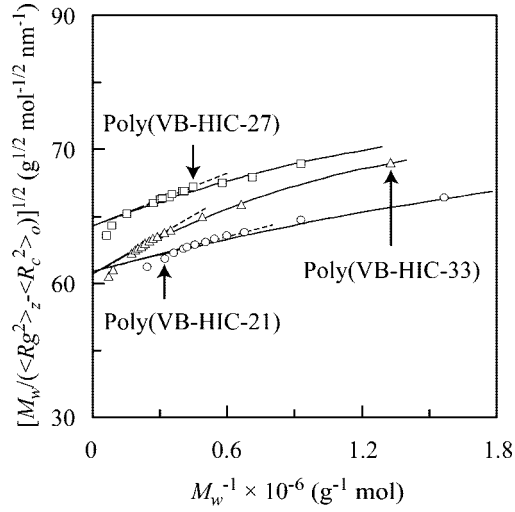

Figure 7. Modified Murakami plots of $(M_w/(\langle R_g^2\rangle_z - \langle R_c^2\rangle_0))^{1/2}$ versus M_w^{-1}, constructed form the experimental $\langle R_g^2\rangle_z$ and $\langle R_c^2\rangle_0$ data for poly(VB-HIC-21), poly(VB-HIC-29), and poly(VB-HIC-32) in THF at 25 °C. The broken lines show a linear region, and the solid lines are theoretical value recalculated by eq 14 with the parameters listed in Table 7.

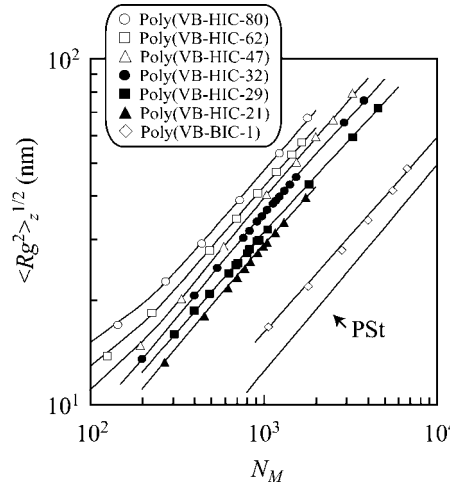

Figure 8. N_M dependence of the measured $\langle R_g^2\rangle_z^{1/2}$ for poly(VB-HIC-N_s) and poly(VB-BIC-1) in THF at 25 °C. The solid lines are the theoretical values for the perturbed wormlike cylinder model using the parameters indicated in Table 7.

Since THF is good solvent for PSt main and PHIC side chains, we take into account the intramolecular excluded-volume effect on $\langle R_g^2\rangle_z$ in the higher N_M region than 10^3. An example is shown in Figure 7 in which the pronounced downward deviations of the plotted points are observed in the high M_w

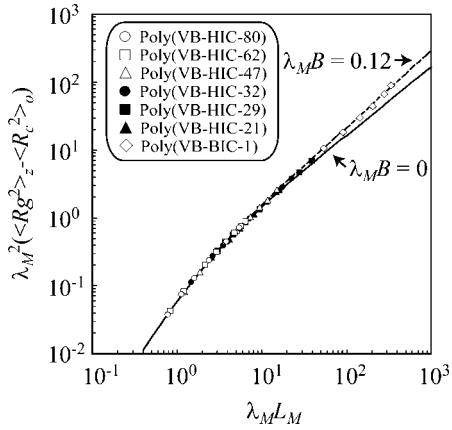

Figure 9. Reduced plots of $\lambda_M^2(\langle R_g^2\rangle_z - \langle R_c^2\rangle_0)$ against $\lambda_M L_M$, constructed from the experimental $\langle R_g^2\rangle_z$ and $\langle R_c^2\rangle_0$ data for poly(VB-BIC-1) and poly(VB-HIC-N_s) in THF. The solid line is the theoretical curves calculated from eq 19 with $\lambda_M B = 0$, and the broken line is the theoretical one calculated from eqs 15−19 with $\lambda_M B = 0.12$.

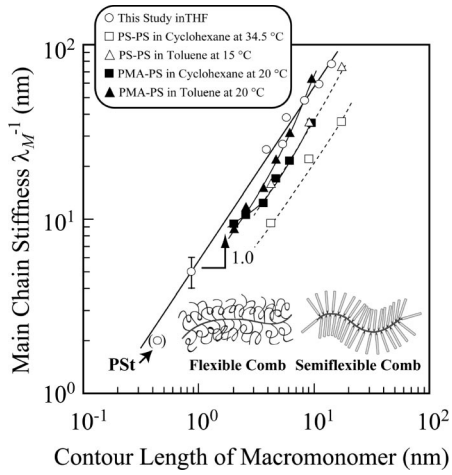

Figure 10. Side chain contour dependence of the main chain stiffness parameter λ_M^{-1}. The reference values[4,8] for the flexible polystyrene polymacromonomer in cyclohexane and toluene and linear PSt[40] are shown for comparison.

region. In the following, we analyzed the $\langle R_g^2\rangle_z$ data with the aid of quasi-two-parameter (QTP) theory[35−37] for the KP chain. In the QTP scheme, the radius expansion factor $\alpha_s = (\langle R_g^2\rangle/\langle R_g^2\rangle_M)^{1/2}$ is a universal function of the scaled excluded-volume parameter $\tilde{z}$ defined by

$$\tilde{z} = \frac{3}{4}K(\lambda_M L_M)z \tag{15}$$

with

$$z = \left(\frac{3}{2\pi}\right)^{3/2}(\lambda_M B)(\lambda_M L_M)^{1/2} \tag{16}$$

and

$$K(\lambda_M L_M) = \frac{4}{3} - 2.711(\lambda_M L_M)^{-1/2} + \frac{7}{6}(\lambda_M L_M)^{-1} \quad \text{for } \lambda_M L_M > 6$$
$$K(\lambda_M L_M) = (\lambda_M L_M)^{-1/2}\exp[-6.611(\lambda_M L_M)^{-1} + 0.9198 + 0.03516(\lambda_M L_M)] \quad \text{for } \lambda_M L_M \le 6 \tag{17}$$

Here, z is the conventional excluded-volume parameter and B is the excluded-volume strength defined by $B = \beta/a^2$ with β and a being the binary cluster integral representing the interaction between a pair of beads and the bead spacing, respectively. Adopting the Domb−Barrett equation[38] for α_s^2, we have

$$\alpha_s^2 = \left[1 + 10\tilde{z} + \left(\frac{70\pi}{9} + \frac{10}{3}\right)\tilde{z}^2 + 8\pi^{3/2}\tilde{z}^3\right]^{2/15}[0.933 + 0.067\exp(-0.85\tilde{z} - 1.39\tilde{z}^2)] \tag{18}$$

The comparison of the experimental data of poly(VB-HIC-32) with theoretical curves (solid line) calculated using eqs 11−18 is shown in Figure 5. The theoretical curve corresponding to $\lambda_M^{-1} = 38$ nm, $M_L = 1.67 \times 10^4$ g mol^{-1} nm^{-1}, $\langle R_c^2\rangle_0^{1/2} = 3.34$ nm, $\delta = 11.6$ nm, and $B = 1.6$ nm is seen to agree closely with the experimental data.

Figure 8 shows N_M dependence of $\langle R_g^2\rangle_z^{1/2}$ for different poly(VB-HIC-N_s)'s in THF at 25 °C. It should be noted that the experimental value of $\langle R_g^2\rangle_z^{1/2}$ increases with N_s at the same N_M, implying that main chain stiffness increases with increasing side rod length. The characteristic parameters of the rod brushes, which are determined by the way mentioned above, are summarized in Table 7. The solid lines in Figure 8 are the theoretical curves calculated from eqs 11−18 with the model parameters listed in Table 7. The experimental N_M dependence of $\langle R_g^2\rangle_z$ for all rod brushes is quantitatively described in terms of the wormlike cylinder model with the end effect.

To demonstrate the validity of the model parameters determined for the present rod brushes, the normalized plot of $\lambda_M^2(\langle R_g^2\rangle_z - \langle R_c^2\rangle_0)$ vs $\lambda_M L_M$, reduced by the stiffness parameter λ_M^{-1}, is reconstructed in Figure 9, where $\lambda_M L_M$ is the number

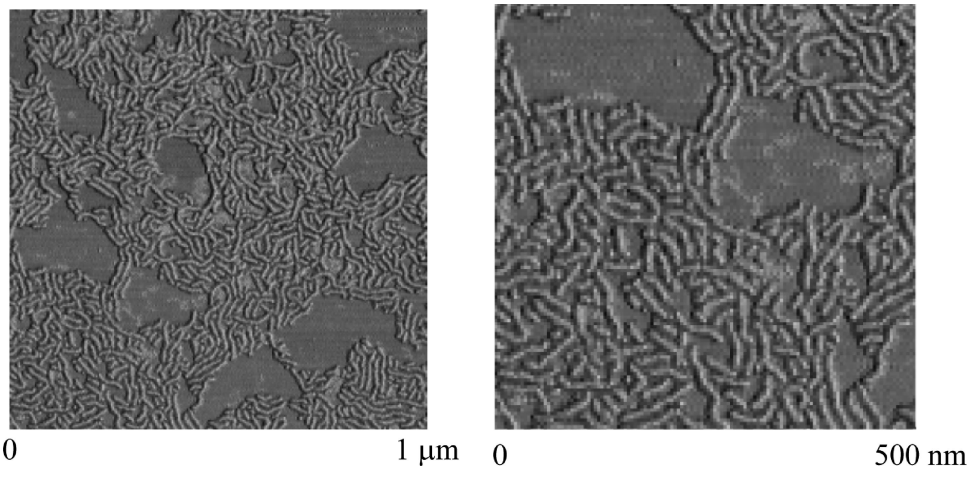

Figure 11. Phase images of SFM measurement for poly(VB-HIC-47) ($M_w = 7.63 \times 10^6$ g mol^{-1}, $M_w/M_n = 1.3_6$) on mica at room temperature.

of Kuhn's segments in the wormlike chain. We note that eq 13 can be rewritten as[39]

$$\lambda_M^2(\langle R_g^2\rangle_z - \langle R_c^2\rangle_0) = \frac{\lambda_M L_M}{6} - \frac{1}{4} + \frac{1}{4(\lambda_M L_M)} - \frac{1}{8(\lambda_M L_M)^2}[1 - \exp(-2(\lambda_M L_M))] \quad (19)$$

Equation 19 implies that $\lambda_M^2(\langle R_g^2\rangle_z - \langle R_c^2\rangle_0)$ is only function of $\lambda_M L_M$ to afford a universal curve before onset of excluded volume effects, irrespective of the type of polymer. One sees clearly in this figure that the experimental data points are superimposed on each other on a line to certify the accuracy of the model parameters determined in the present study.

Figure 10 shows the comparison of the main chain stiffness between brushes with rodlike and flexible side chains. The double-logarithmic plot of the main chain stiffness parameter λ_M^{-1} against the PHIC side chain contour length L_{PHIC} for the rod brushes in THF at 25 °C is shown, together with the reference data for the flexible brushes consisting PSt main and side chains[8] and consisting of polymethacrylate main and PSt side chains,[4] for the comparison. The contour length of the side PSt chain with M_w is calculated by M_w/M_L with the $M_L = 390$ g mol^{-1} nm^{-1}.[8] The values of λ^{-1} of linear PSt (ca. 2 nm[40]) and poly(VB-BIC-1) are also plotted in this figure. It may be very difficult for these linear polymers to determine the side chain contour length. Apparent contour length for the linear polymer may be calculated by assuming a cylinder of uniform density using the experimental value of $\langle R_c^2\rangle_0$ of linear PSt and poly(VB-BIC-1).

There are two important experimental findings to be noted in this figure. First is that the main chain stiffness of the rod combs is higher than that of the flexible combs with the corresponding side contour length, at least in the region of the contour length less than 50 nm, in parallel to the simulation results as mentioned in Introduction. This difference is thought to be due to the larger excluded-volume effects among the side rods than flexible chain. Second is the L_{PHIC} dependence of λ_M^{-1}. One obtains the following scaling relation:

$$\lambda_M^{-1} \propto L_{PHIC}^{1} \propto N_s^{1} \quad (20)$$

This power law exponent value is smaller than that of flexible brushes in a good solvent, toluene. This is most likely due to the higher increase in the number of the contact point between the segments in the flexible side chains than that between the rods. It is also worth noting that the experimental exponent for the rod brush is completely different from that of the theory based on the mean-field approximation as mentioned in Introduction.[24] Further theoretical studies to explain the present experimental results should be desired.

Figure 11 shows the phase image of SFM for poly(VB-HIC-47) ($M_w = 7.63 \times 10^6$ g mol^{-1}, $M_w/M_n = 1.3_6$) on mica at room temperature. Single, high molecular weight, cylindrical brush-like macromolecule with ca. 15 ± 1 nm in a thickness on a mica surface is clearly observed. The thickness in the cross-sectional direction is comparable to two rods (16.7 nm) determined by SAXS measurement in THF.

Conclusion

Dimensional properties of the cylindrical rod brushes are thoroughly studied by static light scattering and small-angle X-ray scattering (SAXS) in THF at 25 °C. The N_s dependence of $\langle R_c^2\rangle_0$ of the rod brushes affords the scaling law of $\langle R_c^2\rangle_0 \propto N_s^{0.87}$. The behavior is explained in terms of the wormlike comb model whose main and side chains have different stiffness parameters. The N_M dependence of $\langle R_g^2\rangle_z$ is also quantitatively described in terms of the wormlike cylinder model taking into account the end effect. The parameters characteristic of the rod brushes in THF solution, such as the main chain stiffness parameter λ_M^{-1}, the molecular weight per unit contour length M_L, and the excluded-volume strength B, are determined and rationalized as a function of the contour length of the side rod. The main chain stiffness increases with the PHIC side rod length (L_{PHIC}) with the relation of $\lambda_M^{-1} \propto L_{PHIC}^{1}$. The main chain stiffness of the rod brush is higher than that of the flexible brush consisting of flexible side chains with the corresponding side chain contour length.

Acknowledgment. Support in part by Grants-in-Aid from the Ministry of Education, Science, Sports and Culture of Japan (16550105) and (19550117), by The Foundation for Japanese Chemical Research, and by Saneyoshi Scholarship Foundation is gratefully acknowledged. The synchrotron radiation experiments were performed at the BL10C in the Photon Factory of the High Energy Accelerator Organization at Tsukuba, Ibaraki, Japan.

References and Notes

(1) Wintermantel, M.; Schmidt, M.; Tsukahara, Y.; Kajiwara, K.; Kohjiya, S. *Macromol. Rapid Commun.* **1994**, *15*, 279.
(2) Tsukahara, Y.; Tsutsumi, K.; Yamashita, Y.; Shimada, S. *Macromolecules* **1990**, *23*, 5201.
(3) Wintermantel, M.; Gerle, M.; Fischer, K.; Schmidt, M.; Wataoka, I.; Urakawa, H.; Kajiwara, K.; Tsukahara, Y. *Macromolecules* **1996**, *29*, 978.
(4) Zhang, B.; Gröhn, F.; Pedersen, J. S.; Fischer, K.; Schmit, M. *Macromolecules* **2006**, *39*, 8440.
(5) Desvergne, S.; Héroguez, V.; Gnanou, Y.; Borsali, R. *Macromolecules* **2005**, *38*, 2400.
(6) Terao, K.; Takeo, Y.; Tazaki, M.; Nakamura, Y.; Norisuye, T. *Polym. J.* **199931**, 193.
(7) Terao, K.; Hokajo, T.; Nakamura, Y.; Norisuye, T. *Macromolecules* **1999**, *32*, 3690.
(8) Hokajo, T.; Terao, K.; Nakamura, Y.; Norisuye, T. *Polym. J.* **2001**, *33*, 481.
(9) Nakamura, Y.; Norisuye, T. *Polym. J.* **2001**, *33*, 874.
(10) Radke, W.; Roos, S.; Stein, H. M.; Müller, A. H. E. *Macromol. Symp.* **1996**, *101*, 19.
(11) Ito, K.; Tomi, Y.; Kawaguchi, S. *Macromolecules* **1992**, *25*, 1534.
(12) Kawaguchi, S.; Akaike, K.; Zhang, Z.-M.; Matsumoto, H.; Ito, K. *Polym. J.* **1998**, *30*, 1004.
(13) Kawaguchi, S.; Maniruzzaman, M.; Katsuragi, K.; Matsumoto, H.; Ito, K.; Hugenberg, N.; Schmidt, M. *Polym. J.* **2002**, *34*, 253.
(14) Ito, K.; Kawaguchi, S. *Adv. Polym. Sci.* **1999**, *142*, 129.
(15) Gunari, N.; Schmidt, M.; Janshoff, A. *Macromolecules* **2006**, *39*, 2219.
(16) Cai, Y.; Hartenstein, M.; Müller, A. H. E. *Macromolecules* **2004**, *37*, 7484.
(17) Djalali, R.; Hugenberg, N.; Fischer, K.; Schmidt, M. *Macromol. Rapid Commun.* **1999**, *20*, 444.
(18) Lee, H-i.; Jakubowski, W.; Matyjaszewski, K.; Yu, S.; Sheiko, S. S. *Macromolecules* **2006**, *39*, 4983.
(19) Braunecker, W. A.; Matyjaszewski, K. *Prog. Polym. Sci.* **2007**, *32*, 93.
(20) Moad, G.; Rizzardo, E.; Thang, S. H. *Aust. J. Chem.* **2005**, *58*, 379.
(21) Fredrickson, G. H. *Macromolecules* **1993**, *26*, 2825.
(22) Zhulina, E. B.; Vilgis, T. A. *Macromolecules* **1995**, *28*, 1008.
(23) Saariaho, M.; Subbotin, A.; Szleifer, I.; Ikkala, O.; Brinke, G. T. *Macromolecules* **1999**, *32*, 4439.
(24) Subbotin, A.; Saariaho, M.; Stepanyan, R.; Ikkala, O.; Brinke, G. T. *Macromolecules* **2000**, *33*, 6168.
(25) Zhang, B.; Fischer, K.; Schmidt, M. *Macromol. Chem. Phys.* **2005**, *206*, 157.
(26) Norisuye, T.; Tsuboi, A.; Teramoto, A. *Polym. J.* **1996**, *28*, 357.
(27) Kikuchi, M.; Kawaguchi, S.; Nagai, K. *Des. Monomers Polym.* **2004**, *7*, 603.
(28) Kawaguchi, S.; Mihara, T.; Kikuchi, M.; Lien, L. T. N.; Nagai, K. *Macromolecules* **2007**, *40*, 950.
(29) Kikuchi, M.; Mihara, T.; Jinbo, Y.; Izumi, Y.; Nagai, K.; Kawaguchi, S. *Polym. J.* **2007**, *39*, 330.
(30) Glatter, O.; Kratky, O. *Small Angle X-ray Scattering*; Academic Press: London, 1982.

(31) Nakamura, Y.; Wan, Y.; Mays, J. W.; Iatrou, H.; Hadjichristidis, N. *Macromolecules* **2000**, *33*, 8323; *Macromolecules* **2001**, *34*, 2018 (for corrections).
(32) Konishi, T.; Yoshizaki, T.; Saito, T.; Einaga, Y.; Yamakawa, H. *Macromolecules* **1990**, *23*, 290.
(33) Benoit, H.; Doty, P. *J. Phys. Chem.* **1953**, *57*, 958.
(34) Murakami, H.; Norisuye, T.; Fujita, H. *Macromolecules* **1980**, *13*, 345.
(35) Yamakawa, H.; Stockmayer, W. H. *J. Chem. Phys.* **1972**, *57*, 2843.
(36) Yamakawa, H.; Shimada, J. *J. Chem. Phys.* **1985**, *83*, 2607.
(37) Shimada, J.; Yamakawa, H. *J. Chem. Phys.* **1986**, *85*, 591.
(38) Domb, C.; Barrett, A. J. *Polymer* **1976**, *17*, 179.
(39) Fujita, H. *Polymer Solutions*; Elsevier: New York, 1990.
(40) Norisuye, T.; Fujita, H. *Polym. J.* **1982**, *14*, 143.

MA800951D